Probabilistic Force Estimation and Event Localization (PFEEL) algorithm

Yohanna MejiaCruz[a,*], **Zhaoshuo Jiang**[a], **Juan M. Caicedo**[b], **Jean M. Franco**[b]

[a]San Francisco State University, 1600 Holloway Ave, San Francisco, CA 94132, United States

[b]University of South Carolina, Columbia SC, 29208, United States

Abstract

Localization of human activity using floor vibrations has gained attention in recent years. In human health technologies, floor vibrations have been recently used to estimate gait parameters to predict a patients' health status. Various methodologies such as using the characteristics of wave traveling (algorithms based on time of arrival) or the properties of structures (Force Estimation and Event Localization, FEEL, algorithm) have been investigated to localize the impact, fall, or step events. This paper presents a probabilistic approach that builds upon the FEEL algorithm to offer the advantage of eliminating the need for a robust experimental setup. The proposed Probabilistic Force Estimation and Event Localization (PFEEL) algorithm provides a probabilistic measure to an event's force estimation and localization using random variables associated with the floor's dynamics. The algorithm can also guide calibration by identifying calibration points that provide the maximum information. This reduces the number of calibration points needed, which has practical benefits during the implementation. In this manuscript, we presented the design, development, and validation of the algorithm.

Keywords

Floor vibrations; Impact location; Event detection; FEEL algorithm; Probabilistic event detection; Bayesian inference; Uncertainty quantification

---

*Corresponding author: mejiacru@sfsu.edu (Y. MejiaCruz).

CRediT authorship contribution statement

Yohanna MejiaCruz: Conceptualization, Methodology, Software, Validation, Formal analysis, Investigation, Data curation, Writing – original draft, Writing – review & editing, Visualization. **Zhaoshuo Jiang:** Conceptualization, Resources, Investigation, Review & editing, Supervision, Project administration, Funding acquisition. **Juan M. Caicedo:** Conceptualization, Methodology, Investigation, Writing – review & editing, Supervision, Project administration, Funding acquisition. **Jean M. Franco:** Software, Resources, Review.

Declaration of competing interest

The authors declare that they have no known competing financial interests or personal relationships that could have appeared to influence the work reported in this paper.

Publisher's Disclaimer: Disclaimers

Publisher's Disclaimer: The content is solely the responsibility of the authors and does not necessarily represent the official views of the National Institutes of Health.

1. Introduction

1.1. Research motivation

Event localization algorithms using floor vibrations have become popular for their widespread applications, including occupant detection [1–5], human health monitoring [6], and security [7]. The use of floor vibrations to track human activity has shown advantages over other technologies, particularly when intrusive technologies such as cameras or wearable sensors are not appropriate or practical (e.g., bathrooms, lockers, or dressing rooms). Identifying human activity using these "smart floors" could help, for example, to reduce cost and energy consumption by controlling the heating and cooling of a building depending on the number of people inside [8]. Similarly, the technology could help track unauthorized activity in isolated areas, buildings, and other facilities for security applications.

A significant portion of the research on smart floors using floor vibrations has focused in recent years on the extraction of gait parameters for health care practices [6,9–12]. This is because previous research has shown that gait parameters can be used as a predictor of frailty, probability of falls [13,14], function loss and even death [9,15–17]. The extraction of these parameters using footstep-induced floor vibrations methods can be advantageous for some particular populations, such as dementia patients, that often forget to wear or charge their wearable devices. In these cases, collecting information from the environment rather than directly from the person is a more suitable approach. The extraction of gait parameters from floor vibrations can be challenging, especially because small variations on gait are hard to capture, and even a small change can have an important outcome as a predictor. For example, previous research has shown that a minimum detectable change of 0.1 m/s can indicate functional decline or change in health status [6,18].

Two of the techniques used on event localization or step event extraction for gait measures are the time of arrival (TOA) and force estimation and event localization algorithm (FEEL). The first group is very popular in the literature for localization [4,5] and include some variations such as time difference of arrival (TDOA), frequency difference of arrival (FDOA), angle of arrival (AOA), and angle constrain time difference of arrival (ATDOA). The TOA approach is based on the estimation of the time that waves take to travel between the source and the sensors [19,20], and the impact's location is estimated based on the time of arrival using at least three sensors. One of the challenges for TOA methods is that the wave propagation is dispersive through the floor, and strong multi-path fading occurs. Changes in vertical rigidity can affect the wave's shape and the propagation velocity for the different frequency components of the wave, making it difficult to estimate the time of arrival accurately [21].

Davis and Caicedo proposed a different type of methodology by designing FEEL [7,22,23]. The algorithm's fundamentals rely on the floor dynamics (input and output relationships) and not on wave propagation. The FEEL algorithm can estimate the location of an event and provide an estimation of the force magnitude. Unlike TOA methods, FEEL requires pre-calibration. The algorithm calculates transfer functions between the forces and the response of the system at specific excitation locations. These transfer functions are unique,

encapsulating the structure's dynamic properties and are not limited by the structural configuration, as long as vibrations signals can be measured. FEEL requires a minimum of two sensors and does not require fully synchronized data acquisition [7].

FEEL establishes the localization of an event as the closest calibrated location, treating space in a discrete fashion (only calibration points), following a deterministic methodology, which is its most substantial limitation, especially in scenarios where an event's localization is needed with high spatial resolution. In those cases, FEEL implementation could require a time-consuming calibration process as the number of necessary calibration points increases. Also, the estimated force and locations from FEEL do not include an estimate of their uncertainty.

In this paper, we propose a reformulation of the FEEL algorithm to overcome its limitations. The new formulation is performed in a probabilistic fashion to provide an estimation of the uncertainty of the identified forces and their locations. A significant portion of the literature in structural dynamics and materials has focused on measuring the uncertainty of the dynamic systems [24–29]. The need to measure the uncertainty arises from the errors of constructing theoretical models, including inexact representation of boundary conditions and incomplete data relative to the model complexity [28]. Also, constructing probabilistic models allows to include expert knowledge obtained from similar systems to the inference process [28,30]. The probabilistic FEEL algorithm employs a theoretical response formulation, which inherently is a source of uncertainty but allows making predictions in locations with no experimental information. PFEEL uses a continuous model of the structure in terms of space and can identify the location of an event, even if its location has not been used for calibration. Also, unlike TOA methods, PFEEL is based on the dynamics of the structure, and variations in vertical rigidity are intrinsically considered when building the transfer functions of the structural system. As long as acceleration signals can be measured with a reasonable signal-to-noise ratio, and the room's structural configuration or mass layout has not changed dramatically, these relationships will not change; thus, PFEEL's calibration is not affected.

The first part of this manuscript contains a short review of FEEL's theoretical background, followed by the introduction of the newly proposed method. The rest of the article provides a detailed description of the proposed method and its validation through the use of a simply supported beam model.

1.2. FEEL theoretical background

The steps to apply FEEL are presented in Fig. 1. The calibration in the sequence focuses on estimating the transfer functions $(\widehat{TF})$ between an applied force P and an acceleration response R. The transfer functions are obtained using:

$$\widehat{TF}_{P,R}(f) = \frac{\hat{S}_{P,R}(f)}{\hat{S}_{P,P}(f)}; \quad \widehat{TF}_{R,P}(f) = \frac{\hat{S}_{R,R}(f)}{\hat{S}_{R,P}(f)}; \tag{1}$$

$$\widehat{TF}(f) = \frac{\widehat{TF}_{P,\,R}(f) + \widehat{TF}_{R,\,P}(f)}{2} \tag{2}$$

Here, $\hat{S}$ is the cross and auto power spectral density between P and R [23,31,32]. For a specific event location i and sensor location ϵ, the transfer function associated with the input/output is represented by $\widehat{TF}_{i\epsilon}$ as a function of the frequency f, as shown in Eq. (3).

Once a particular event is identified by a spike on the acceleration in the operation stage, forces are first estimated at all calibration locations and then the impact location is identified by comparing the force estimates. The estimation of the forces in Fig. 1 is the reconstruction of the force using the TFs from the calibration stage, and accelerations ($\ddot{R}(t)$) from a new event

$$\widehat{F}_{i\epsilon}(t) = \text{IFFT}\left(\frac{\text{FFT}(\ddot{R}(t)_\epsilon)}{\widehat{TF}_{i\epsilon}(f)}\right) \tag{3}$$

Where FFT and IFFT represent the Fast Fourier Transform and its inverse, respectively, and $\widehat{F}_{i\epsilon}(t)$ represents the force estimates at i given the acceleration at ϵ.

The location of the event in Fig. 1 is estimated using the similarity between force estimates from different sensors. With a selected window of force estimates $\widehat{F}_{i,\,\epsilon}(t)$, FEEL calculates the Pearson product-moment correlation coefficient ($\rho_{\epsilon_m \epsilon_n}$) between sensors ϵ_m and ϵ_n (Eq. (4)), where COV is the covariance between the forces of sensors ϵ_m and ϵ_n, and σ_m and σ_n are their standard deviations. The result is the matrix of normalized coefficients presented in Eq. (5), where $\{L_i\}$ is the maximum value obtained per location i.

$$\rho_{\epsilon_m \epsilon_n} = \frac{COV(\epsilon_m, \epsilon_n)}{\sqrt{\sigma_{\epsilon_m} \sigma_{\epsilon_n}}} \tag{4}$$

$$\{L_i\} = \max \begin{bmatrix} 0 & \rho_{\epsilon_1 \epsilon_2}\left(\widehat{F}_{i,\,\epsilon_1}(t), \widehat{F}_{i,\,\epsilon_2}(t)\right) & \cdots & \rho_{\epsilon_1 \epsilon_n}\left(\widehat{F}_{i,\,\epsilon_1}(t), \widehat{F}_{i,\,\epsilon_n}(t)\right) \\ & 0 & \cdots & \rho_{\epsilon_2 \epsilon_n}\left(\widehat{F}_{i,\,\epsilon_2}(t), \widehat{F}_{i,\,\epsilon_n}(t)\right) \\ & & \ddots & \vdots \\ \text{sym.} & & & 0 \end{bmatrix} \tag{5}$$

FEEL identifies the event location as the location i with the maximum value of $\{L_i\}$. The force magnitude estimation is then calculated by using the average between the force estimates at location i [7].

1.3. Contribution of this paper

One of the challenges associated with FEEL is that the force estimates are accurate when events happen in the vicinity of a calibration point. Accuracy is reduced as events occur far from these points because the transfer function between the impact location and the sensors

is not well represented by the calibration process. Furthermore, FEEL does not provide uncertainty estimation on the force or the location.

A new probabilistic approach based on FEEL is proposed to obtain the location of an event (e.g., footstep or fall) between points of calibration. This is achieved by modeling the transfer functions between impact and response locations as a hyper-surface. This model is determined probabilistically following the fundamentals of the FEEL algorithm but by considering the response parameters as random variables and updating their distributions using Bayesian Inference. The Probabilistic-FEEL (PFEEL) algorithm has several advantages over FEEL: (1) it reduces the necessity of extensive initial system identification tests by reducing the number of calibration points; (2) it can be used to locate impacts where no pre-calibration has taken place, and (3) it estimates the uncertainty of event locations and estimated forces.

2.   Probabilistic Force Estimation and Event Localization (PFEEL) algorithm

The transfer function between forces at a particular location and acceleration records collected by sensors placed at an another specific location is unique. We take advantage of this spatial variation to identify the location of the impact event. To do so, it requires a calibration process where impact hammers are used to excite the structure at calibration points. Given the discrete nature of the calibration points, the calibration data provides discrete information. However, the transfer function, as a function of space, will be needed to locate and estimate forces if an impact occurs outside these calibration points. To accomplish this task, PFEEL employs a response model to simulate the dynamics of the structure with forces at any location. This model is then used to estimate the structure's transfer function at any location of interest with coordinates (x,y). We refer to this response model as the probabilistic response model (PREP).

2.1.   Probabilistic response model (PREP)

Without any lost of generality, the following paragraphs describes the response model of a one-dimensional linear system (e.g. beam) for the sake of simplicity. Here, space is determined by one variable only (x) instead of two variables (x, y). The total response of a one-dimensional linear system, such as the beam, with classical damping can be represented by the superposition of the contributions of each orthogonal mode [33], using the expression:

$$u(x,t) = \sum_{r=1}^{N} \phi_n(x) \times q_n(t) \tag{6}$$

With N modes contributing to the response, with $q_n(t)$ as the solution in generalized coordinates of the uncoupled SDOF system and $u(x, t)$ as the total response.

For uncoupled differential equations in $q_n(t)$, an impulse with amplitude p_o centered at $t = \tau$, induces free vibration due to initial velocity and displacement, then:

$$q_n(t) = \frac{P_n}{M_n \omega_d} e^{-\zeta_n \omega_n (t - \tau)} \sin[\omega_d(t - \tau)] \tag{7}$$

Where ζ_n, ω_n and ω_d are the damping, natural angular frequency and damped angular frequency associated to the nth mode, respectively. $M_n = \int_o^L m(x)\phi(x)^2 dx$, and $P_n = \int_o^L p_o(x,t)\phi(x)dx$, where $m(x)$, $p_o(x, t)$ and $\phi(x)$ are the modal mass, modal force and mode shapes, respectively. The mode shapes depend on the structure and boundary conditions. For a simply supported Euler–Bernoulli beam with a length L and constant cross section, for example, the normal modes are given by the equation:

$$\phi_n(x) = \sin\left(\frac{n\pi x}{L}\right) \tag{8}$$

Similar to Eq. (6), and Eq. (8), the total response of a two-dimensional simply supported system can be expressed as a superposition of modes using:

$$R(x, y, t) = \sum_{k = 1, 2, 3..}^{\infty} Z(x, y)_k q_k(t) \tag{9}$$

where $Z(x, y)$ represents the shape function and $q_k(t)$ are the uncoupled differential equations.

The shape function of the PREP model is defined by Eq. (10), which is the derivation of the vibrational modes of a simply supported steel plate [34,35]. Note that the shape function assumes a simply supported boundary condition in this study. However, the shape function can be changed for any other function that best represents the system's vibration.

$$Z_k(x, y) = \sin\left(\frac{k\pi x}{Lx}\right)\sin\left(\frac{k\pi y}{L_y}\right) \tag{10}$$

With k replacing the combination of the mode number (n) in each direction $k = (n_x, n_y)$, and where L_x and L_y are the total length in the x and y axis, respectively. The uncoupled differential equation for the k mode is given by

$$q_k(t) = \frac{P_k}{M_k}\frac{1}{\omega_{d, k}} e^{(-\zeta \omega_k t)} \sin(\omega_{d, k}(t - \tau)) \tag{11}$$

With:

$$P_k = \int_0^{Lx} \int_0^{Ly} P(x, y, t) \times Z_k(x, y)dxdy$$
$$M_k = \int_0^{Lx} \int_0^{Ly} M(x, y) \times Z_k(x, y)^2 dxdy \tag{12}$$

2.2. Probabilistic formulation of the response using Bayes

PFEEL requires an estimation of the modes of the system ($\phi_n(x)$). However, given that an exact estimation may be difficult to get, the PREP model and its parameters are the most significant sources of uncertainty. As mentioned earlier, the formulation of the responses is made using the Bayes rule in Eq. (13).

$$P(\theta \mid D) = \frac{P(\theta)P(D \mid \theta)}{P(D)} \tag{13}$$

Where $\theta = \left\{ f_{n_k}, \zeta_k, C_i \right\}$ with f_{n_k} as the natural temporal frequencies, and ζ_k the damping ratios for each mode considered. A scale correction factor "C_i" that accounts for the difference between the mode shapes identified from the numerical model and from experimental data was also included as an unknown quantity (see Eqs. (10) and (14)).

$$Z_k(x, y) = C_i \sin\left(\frac{k\pi x}{Lx}\right) \sin\left(\frac{k\pi y}{Ly}\right) \tag{14}$$

For the model to better represent the phenomenon under observation, experimental data collected from the system is used to inform the model. D in Eq. (13) represents the information obtained from the experimental testing. The experimental data is a frequency response function matrix of size $q \times e$ for q impacts and e sensors. The TF's amplitude (r) and phase (ϕ) components are the observations of the model $D = \{D_1, D_2\}$, with $D_1 = \log(r)$ and $D_2 = \phi$.

In the Bayesian formulation, $P(\theta)$ is the prior distribution of the model parameters, representing the prior knowledge about the parameters. For example, the authors believe that the frequencies associated with the different mode shapes will follow normal distributions. However, not much information regarding the proper distributions of the damping ratio and the scale parameters is available. In the last case, the distributions for ζ_n and C_i have been selected using the maximum entropy criteria [36–38]. The parameters' prior distributions were selected as $f_{n_k} \sim N\left(\mu = f_{n_{k_0}}\right)$; $\zeta_k \sim Exp\left(\lambda = 1/\zeta_{k_0}\right)$; and $C_i \sim U(a = c_0, b = c_i)$.

$P(D|\theta) = P(D_1|\theta)P(D_2|\theta)$ represents the conditional probability of the parameters under the observations. In this study measurement errors are simulated using independent zero-mean normal random numbers for each sensor and small modeling errors are expected. Therefore, the likelihood function will follow a Gaussian distribution. Experimental applications might not follow a normal distribution and should be further studied as discussed by other authors [39,40]. Given the two sets of observations D_1 and D_2, the likelihood function for the two sets of observations is defined as:

$$P(D_1 \mid \theta) = \prod_{i=1}^{n} \frac{1}{\sigma_r \sqrt{2\pi}} \times \exp\left[-\frac{1}{2} \frac{(\log(r_i) - \log(\hat{r}_i)(\theta))^2}{\sigma_r^2} \right] \tag{15}$$

$$P(D_2 \mid \theta) = \prod_{i=1}^{n} \frac{1}{\sigma_\phi \sqrt{2\pi}} \times \exp\left[-\frac{1}{2} \frac{\left(\phi_i - \hat{\phi}_i(\theta)\right)^2}{\sigma_\phi^2}\right] \tag{16}$$

Where σ_r and σ_ϕ are the standard deviation of the likelihood, and are considered unknown random variables. $\log(\hat{r}_i)(\theta)$ and $\hat{\phi}_i(\theta)$ are the log-amplitude and phase predictions, $\log(r_i)$ and ϕ_i are the ith log-amplitude and phase observations, n is the total number of observations and $\theta = \{f_{n_k}, \zeta_k, C_i, \sigma_r, \sigma_\phi\}$.

To predict an unknown observable, a similar logic as the one presented in Eq. (13) is followed. Before the data D is considered, the distribution of the unknown observation is:

$$P(D) = \int P(D, \theta)d\theta = \int P(\theta)P(D \mid \theta)d\theta \tag{17}$$

Eq. (17) is the prior predictive distribution not conditioned to previous observations [41,42]. When D is observed, the prediction of an unknown observable $\tilde{D}$ can be obtained using:

$$P(\tilde{D} \mid D) = \int P(\tilde{D}, \theta \mid D)d\theta = \int P(\tilde{D} \mid \theta, D)P(\theta \mid D)d\theta = \int P(\tilde{D})P(\theta \mid D)d\theta \tag{18}$$

Eq. (18) can be used to predict the response at any location. The probabilistic model generates predictions of the amplitude and the phase under θ. Thus, we can obtain an approximation of the posterior distributions of the random variables and distributions of the unknown observables — TFs at any location.

3. PFEEL algorithm design

As shown in Fig. 2, the PFEEL algorithm is composed of three consecutive stages, namely probabilistic transfer function estimations (PTF), probabilistic force estimations (PFE), and probabilistic event localization (PEL).

3.1. Probabilistic transfer functions (PTF)

The first stage focuses on constructing the probabilistic transfer function (PTF) estimates at any location (x, y). These locations generate the hypersurface of transfer functions. In this stage, the PREP model (Section 2) is excited at multiple locations with coordinates (x, y), and the system's response is recorded at the location of the sensors (ϵ). These TFs are obtained using Eq. (19). Notice that $\widehat{TF}$ and $\hat{S}$ are functions not only of the space (x, y) but of the frequency; however, f is dropped in the forthcoming equations for simplicity.

$$\widehat{TF}_{P_{(x,y)}R_\epsilon} = \frac{\widehat{TF}_{P_{(x,y)}R_\epsilon} + \widehat{TF}_{R_\epsilon P_{(x,y)}}}{2} \tag{19}$$

where, $\widehat{TF}_{P_{(x,y)}R_\epsilon} = \dfrac{\hat{S}_{P_{(x,y)}R_\epsilon}}{\hat{S}_{RR_\epsilon}}$, $\widehat{TF}_{R_\epsilon P_{(x,y)}} = \dfrac{\hat{S}_{PP_{(x,y)}}}{\hat{S}_{R_\epsilon P_{(x,y)}}}$. $\hat{S}_{P_{(x,y)}}$ is the power spectral density

of the force P applied at location (x,y), and $\hat{S}_{R_\epsilon}$ the power spectral density of the response R

measured at a sensor location ϵ. The rest of the variables represent the cross-power spectral

densities between these. Granted, $0 < x < L_x$ and $0 < y < L_y$, where L_x and L_y are the largest

physical dimension where a sensor can be positioned in axis x and y, respectively.

Notice that Eqs. (2) and (19) have a similar convention for power and cross-power spectral

density functions, only that $\hat{S}_{R_\epsilon}$ are probability distributions as a function of the random

variables, as shown in Section 2.2, and as a function of x and y. Also, $\widehat{TF}_{PR}$ is a continuous

probability distribution obtained using Eq. (18), where $\widetilde{D}_{P_{(x,y)}R_\epsilon}$ are the predictions of the

amplitude $\tilde{r}_{P_{(x,y)}R_\epsilon}$, and the phase $\tilde{\phi}_{P_{(x,y)}R_\epsilon}$ in the space. The complex transformation is

made using $\widehat{TF}_{P_{(x,y)}R_\epsilon} = \tilde{r}_{P_{(x,y)}R_\epsilon}\left(\cos\left(\tilde{\phi}_{P_{(x,y)}R_\epsilon}\right) + i\sin\left(\tilde{\phi}_{P_{(x,y)}R_\epsilon}\right)\right)$.

3.2. Probabilistic force estimates (PFE)

The second stage of the algorithm focuses on estimating the impact force distributions using new acceleration data $\ddot{R}(t)$ captured by the sensors ϵ. With the spatial transfer functions $\widehat{TF}_{P_{(x,y)}R_\epsilon}$, the force estimations for each sensor can be obtained using:

$$\hat{P}(x,y,t)_\epsilon = \text{IFFT}\left(\frac{\text{FFT}\left(\ddot{R}_\epsilon(t)\right)}{\widehat{TF}_{P_{(x,y)}R_\epsilon}}\right) \tag{20}$$

$\hat{P}(x,y,t)_\epsilon$ are distributions of the force estimates for locations (x,y) using sensor ϵ in the time domain.

3.3. Event localization (EL)

The third and final stage of the algorithm focuses on the localization of the event. The estimation of the localization is made by comparing the force estimates obtained from Section 3.2. The impact force of a specific event captured by all sensors should theoretically be the same, so the impact location can be determined by comparing the different force estimates' distributions. In this study, the Kolmogorov Smirnov (K-S) test, which compares the similarity of cumulative distributions functions (CDF) [43], is used to determine the location (x,y) where the force estimates' distributions in all sensors (ϵ) are approximately equal.

The K-S test is a type of hypothesis test where the null hypothesis assumes that there are no differences between the observations and the theoretical distribution. The test compares an observed and a theoretical cumulative distribution of a random sample. Instead of comparing between theoretical and observed cumulative distributions, it is adopted in the proposed PFEEL algorithm to establish an agreement between the CDFs of different pairs of samples. For this end, the K-S two-sample test is used, and it is calculated using Eq. (21), where e is the total number of sensors, and i and j are pair of sensors.

$$KS_{ij}(x, y) = \max\left| \iint \hat{P}(x, y, t)_{\epsilon = i} dP\, dt - \iint \hat{P}(x, y, t)_{\epsilon = j} dP\, dt \right| \tag{21}$$

The combinations i-j of pair of sensors should not include repetitions. Thus, the formulation of the final statistics for each location (x, y) is the average of KS values considering all available sensors and can be calculated using Eq. (22). Herein, the statistics Γ is a continuous function in the space. The location of the event is selected as the location (x, y) where Γ is minimum.

$$\Gamma(x, y) = \frac{2!(e-2)!}{e!} \sum_{i=1}^{i=e} \sum_{j=i+1}^{j=e} KS_{ij}(x, y) \tag{22}$$

4. Numerical validation

A simply supported beam model with the properties presented in Table 1 is used to demonstrate the implementation of the proposed PFEEL algorithm. In this example, the beam was hit on five different locations using an impulse force with magnitude of $p_o = 444$ N, as shown in Fig. 3. The response of the system was also measured in the same locations. Fig. 4 shows the amplitude and phase of the frequency response function matrix generated using Eq. (1). The locations of the hit (P_x) and sensors (ϵ) were selected as x, $\epsilon_x = \{0.03, 1.04, 2.06, 3.07, 4.09\}$ m. Notice that in this example, the beam is analyzed as a one-dimensional structure to clearer showcase the implementation of the algorithm.

The frequency response function (FRF) measurements in Fig. 4 are observations $D = \{log(r), \phi\}$, $\log(r)_{P_X R_\epsilon} = \log\left(\left| FRF_{P_X R_\epsilon} \right|\right)$ and $\phi_{P_X R_\epsilon} = \angle\left(FRF_{P_X R_\epsilon} \right)$, where P_x and R_ϵ are the impact force and the sensors response at the actual impact locations.

4.1. Markov chain Monte Carlo simulations

The next part of the validation is the probabilistic formulation of the response, which includes the definition of the prior distributions of the random variables as addressed in Section 2.2, and the inference using Eqs. (13)–(16).

To reach a reasonable approximation of the posterior distributions, Markov Chain Monte Carlo Simulations, particularly the Metropolis–Hasting sampler [44–46] were used. Given that it is not possible to observe convergence with a single sequence, a convergence diagnostic using the potential scale reduction factor (PSRF) [47] was performed. The Fig. 5 shows the convergence of the random variables reached at 10^4 samples. The posterior distributions of the random variables are presented in Fig. 6.

The predictions of the transfer functions at any location x were compared to the newly collected experimental data in those same locations to check the fit's adequacy. Figs. 7 and 8 shows the prediction of the transfer functions using their amplitude and phase. The gray band in both figures represents the 95% credible intervals with the mean represented by the dashed line. The continuous line in both plots represents experimental data collected at that

location to validate the prediction. The results indicate that the observed data lines inside the region of higher probability.

4.2. Force estimation

Now that the whole space of the beam has been characterized in a probabilistic fashion, the hyperspace of transfer functions can be used to establish the localization of a new event (Section 3.2).

The beam was excited to test the ability of the model to detect the localization of the event. New acceleration data collected from the sensors, and the hyperspace of transfer functions from the previous step were used to rebuild the force estimates distributions as shown in Fig. 9. Notice how the force estimates, similar to the transfer function estimates, are represented by distributions with the mean and the 95% credible interval. The actual location of the event occurred at 3.58 m. The results demonstrate, for example, how the force estimate distributions at location 2.06 m (first item-second row) show that the distributions are very different between sensors. In contrast, the force estimates of location 3.58 m (first item-third row) show that the distributions are aligned for all sensors. In addition to the distributions, the magnitude of the force estimated in all the locations is also presented in Fig. 9 in the small subplots on the left corner. The force's histogram in each location was obtained by integrating the force distributions of all sensors at the time of the impact ($t = $ t). As can be observed, the distribution of the force in the exact location of the event ($x = 3.58$ m) contains the real force estimate.

4.3. Event localization

Each location on the hyperspace will contain as much force estimate distributions as the number of sensors available. The localization of the event is defined using the similarity between distributions for all sensors at each location, as explained in Section 3.3. For any new impact location with coordinates (x, y), the prediction of the impact location is a minimization problem of the statistics, Γ, of Eq. (22). Notice in Fig. 9 how the force estimate distributions in the location of the event are aligned for all the sensors. This indicates that the comparison of the force estimate distributions will reflect that similarity between sensors.

Fig. 10 presents the optimization results of Eq. (22) for an impact at $x = 3.58$ m. The initial guess of the optimization was selected as $x = 2.54$ m for this exercise. The correct localization of the event from the optimization was $x = 3.56$ m, 2 cm from the actual impact location, as it can be observed in Fig. 10.

Note that although the FRF matrix used for calibration does not contain a calibration point close to the location of this impact, the algorithm was able to establish the localization with a minimal margin of error, demonstrating the robustness of the proposed algorithm. Although these results confirm that the algorithm can reduce the error in the predictions without extensive calibration tests, it is worth highlighting the important role of the experimental data in informing the model. To establish the best locations to hit and improve the accuracy of the estimations, we used a feature of the algorithm that informs where to hit next to reduce the uncertainty on the predictions and improve the optimization.

5. PFEEL — Calibration

PFEEL requires calibration to establish a model of the structure that can be used to estimate event locations. The goal is to develop a calibration process that could be implemented in a reasonable time. Calibration is only required once, and recalibration may be needed if there are significant changes to the structure (e.g., mass or stiffness changes).

One of the advantages of the proposed PFEEL algorithm is its capacity to inform where the new excitation should take place to reduce the uncertainty of the estimations. With this feature, the amount of experimental data required to accomplish a level of precision can be greatly reduced.

The process to establish the localization of a new hit is an iterative process showed in Fig. 11. After an initial hit event is collected $\Theta(i = 1)$, the algorithm finds the localization with the highest uncertainty in the transfer function space $\widehat{TF}_{(x, y)}R_\epsilon$ using the statistics

$$\Lambda(x, y) = \delta \int \upsilon(x, y, f) \, df \tag{23}$$

where $\upsilon(x, y, f) = Var\left(\widehat{TF}(f)_{P_{(x, y)}R_\epsilon}\right)$ and δ is a normalization constant. The next hit location is selected as the location (x, y) where Λ is maximum. This process is repeated until one of the predefined thresholds, namely, maximum number of hits (N_{max}) or a maximum acceptable variance (Λ_{max}) has been reached.

To establish the next calibration location, we implemented the iterative process in the simply supported beam. The results are presented in Figs. 12 and 13. In Fig. 12 the initial calibration was made at $x = 0.03$ m, and the location of higher uncertainty in the estimations using Eq. (23) was established as the location $x = 4.09$ m. With these results, the next calibration location was selected as $x = 4.09$ m in the next iteration and so on.

Fig. 13 shows the heat map of $\Lambda(x)$ for each iteration. The location with color white is the location with higher uncertainty, and the marker for the next calibration point. The location with the highest uncertainty of the prediction is added as an observation in the next iteration. These plots demonstrate how the stabilization is reached when the number of hits is equal to the number of locations made available for prediction. This behavior is expected and indicates that the minimum uncertainty is obtained if experimental data for all the possible locations is available. As it may not be feasible in practice to excite all the possible locations, a maximum number of calibrations or a threshold of maximum variation Λ should be provided to balance the sufficient level of uncertainty and the efforts needed for the calibration process.

6. Conclusions

The PFEEL algorithm provides a probabilistic estimation of the event location by modeling the system's response as a function of random variables, representing the dynamics of the floor. Building upon and overcoming the challenges of the deterministic FEEL algorithm, the PFEEL algorithm provides a measure of uncertainty on the estimations and reduces

the necessity of extensive experimental calibration tests. These unique characteristics are especially beneficial in cases where the identification of the event localization should be provided with a low margin of error, such as in the case of gait parameter extraction.

To validate the algorithm, a simply supported beam model was used. The localization of the actual impact and the event's location, determined by the algorithm, showed a marginal error of 2 cm (in a 5 m beam), demonstrating that PFEEL can localize the event in locations where even no experimental data has been collected with a low margin of error. The validation results also showed that the distribution of the force provided by PFEEL contains the true value of the force magnitude, indicating that the model can provide a measure of the estimation with the associated uncertainty of the model and the random variables.

The PFEEL algorithm establishes the localization of the event using a probabilistic optimization process. Any optimization method can be used to minimize the function $\Gamma(x, y)$. This optimization methodology should allow an efficient exploration of the solution space.

PFEEL is also capable of informing the next calibration location to reduce the uncertainty in the force and location estimations. PFEEL's calibration is an optimization problem of the function $\Lambda(x, y)$, which allows the user to reduce or extend their experimental setup accordingly.

PFEEL uses the system identification process to provide an initial guess of the random variables, namely, natural frequencies, damping ratios, and mode shapes, to define the prior distributions. The authors recommend implementing an accurate system identification methodology to obtain correct estimations of the mode shapes and natural frequencies. Additionally, if other system changes are included, such as added masses, modified boundary conditions, or changes in the initial real sensors location, a complete re-calibration may be necessary.

Acknowledgments

References

[1]. Drira S, Pai SG, Reuland Y, Olsen NF, Smith IF. Using footstep-induced vibrations for occupant detection and recognition in buildings. Adv Eng Inform 2021;49:101289.

[2]. Pan S, Yu T, Mirshekari M, Fagert J, Bonde A, Mengshoel OJ, Noh HY, Zhang P. Footprintid: Indoor pedestrian identification through ambient structural vibration sensing. Proc ACM Interact Mobile Wearable Ubiquitous Technol 2017;1(3):1–31.

[3]. Oguchi K, Iwago M. Human localization in the home by using floor-mounted acceleration sensors. In: 2018 IEEE sensors. IEEE; 2018, p. 1–4.

[4]. Li F, Clemente J, Valero M, Tse Z, Li S, Song W. Smart home monitoring system via footstep induced vibrations. IEEE Syst J.

[5]. Mirshekari M, Fagert J, Pan S, Zhang P, Noh HY. Step-level occupant detection across different structures through footstep-induced floor vibration using model transfer. J Eng Mech 2020;146(3):04019137.

[6]. MejiaCruz Y, Franco J, Hainline G, Fritz S, Jiang Z, Caicedo JM, Davis B, Hirth V. Walking speed measurement technology: a review. Curr Geriatr Rep 2021;1–10.

[7]. Davis BT, Caicedo JM, Hirth VA. Force estimation and event localization (feel) of impacts using structural vibrations, Journal of Engineering Mechanics 10.1061/(ASCE)EM.1943-7889.0001890.

[8]. Zhang J, Lutes RG, Liu G, Brambley MR. Energy savings for occupancy-based control (Obc) of variable-air-volume (Vav) systems. Tech. rep, Richland, WA (United States: Pacific Northwest National Lab.(PNNL; 2013.

[9]. Kessler E, Malladi VVS, Tarazaga PA. Vibration-based gait analysis via instrumented buildings. Int J Distrib Sens Netw 2019;15(10):1550147719881608.

[10]. Fagert J, Mirshekari M, Pan S, Zhang P, Noh HY. Structural property guided gait parameter estimation using footstep-induced floor vibrations. In: Dynamics of civil structures, vol. 2. Springer; 2020, p. 191–4.

[11]. Dong Y, Zou JJ, Liu J, Fagert J, Mirshekari M, Lowes L, Iammarino M, Zhang P, Noh HY. Md-vibe: physics-informed analysis of patient-induced structural vibration data for monitoring gait health in individuals with muscular dystrophy. In: Adjunct proceedings of the 2020 ACM international joint conference on pervasive and ubiquitous computing and proceedings of the 2020 ACM international symposium on wearable computers. 2020, p. 525–31.

[12]. Fagert J, Mirshekari M, Pan S, Zhang P, Noh HY. Gait health monitoring through footstep-induced floor vibrations. In: Proceedings of the 18th international conference on information processing in sensor networks. 2019, p. 319–20.

[13]. Aziz O, Musngi M, Park EJ, Mori G, Robinovitch SN. A comparison of accuracy of fall detection algorithms (threshold-based vs. machine learning) using waistmounted tri-axial accelerometer signals from a comprehensive set of falls and non-fall trials. Med Biol Eng Comput 2017;55(1):45–55. [PubMed: 27106749]

[14]. Ren L, Peng Y. Research of fall detection and fall prevention technologies: A systematic review. IEEE Access 2019;7:77702–22.

[15]. Rodríguez-Molinero A, Herrero-Larrea A, Miñarro A, Narvaiza L, Gálvez-Barrón C, León NG, Valldosera E, de Mingo E, Macho O, Aivar D, et al. The spatial parameters of gait and their association with falls, functional decline and death in older adults: a prospective study. Sci Rep 2019;9(1):1–9. [PubMed: 30626917]

[16]. Thaler-Kall K, Peters A, Thorand B, Grill E, Autenrieth CS, Horsch A, Meisinger C. Description of spatio-temporal gait parameters in elderly people and their association with history of falls: results of the population-based cross-sectional kora-age study. BMC Geriatr 2015;15(1):32. [PubMed: 25880255]

[17]. Mirshekari M, Fagert J, Bonde A, Zhang P, Noh HY. Human gait monitoring using footstep-induced floor vibrations across different structures. In: Proceedings of the 2018 ACM international joint conference and 2018 international symposium on pervasive and ubiquitous computing and wearable computers. 2018, p. 1382–91.

[18]. Goldberg A, Schepens S. Measurement error and minimum detectable change in 4-meter gait speed in older adults. Aging Clin Exp Res 2011;23(5):406–12. [PubMed: 22526072]

[19]. Poston JD, Buehrer RM, Tarazaga PA. Indoor footstep localization from structural dynamics instrumentation. Mech Syst Signal Process 2017;88:224–39.

[20]. Woolard AG, Tarazaga PA. Applications of dispersion compensation for indoor vibration event localization. J Vib Control 2018;24(21):5108–17.

[21]. Mirshekari M, Pan S, Zhang P, Noh HY. Characterizing wave propagation to improve indoor step-level person localization using floor vibration. In: Sensors and smart structures technologies for civil, mechanical, and aerospace systems 2016, vol. 9803. International Society for Optics and Photonics; 2016, 980305.

[22]. Davis BT. Characterization of human-induced vibrations [Ph.D. thesis], University of South Carolina; 2016.

[23]. Davis BT, Caicedo JM. Impact force estimation and event localization (4 2017).

[24]. Huang Y, Shao C, Wu B, Beck JL, Li H. State-of-the-art review on bayesian inference in structural system identification and damage assessment. Adv Struct Eng 2019;22(6):1329–51.

[25]. Catanach TA, Beck JL. Bayesian system identification using auxiliary stochastic dynamical systems. Int J Non-Linear Mech 2017;94:72–83.

[26]. Yuen K-V. Bayesian methods for structural dynamics and civil engineering. John Wiley & Sons; 2010.

[27]. Lam HF, Katafygiotis LS, Mickleborough NC. Application of a statistical model updating approach on phase i of the iasc-asce structural health monitoring benchmark study. J Eng Mech 2004;130(1):34–48.

[28]. Beck JL, Katafygiotis LS. Updating models and their uncertainties. i: Bayesian statistical framework. J Eng Mech 1998;124(4):455–61.

[29]. Katafygiotis LS, Papadimitriou C, Lam H-F. A probabilistic approach to structural model updating. Soil Dyn Earthq Eng 1998;17(7–8):495–507.

[30]. MejiaCruz Y Probabilistic multilevel constitutive model of the compressive strength of hardened cement paste reinforced with Mwcnts [Ph.D. thesis], University of South Carolina; 2018.

[31]. Ewins DJ. Modal testing: Theory, practice and application. John Wiley & Sons; 2009.

[32]. Bendat JS, Piersol AG. Random data: Analysis and measurement procedures, vol. 729. John Wiley & Sons; 2011.

[33]. Chopra A Dynamics of structures. Pearson Education; 2012, URL https://books.google.com/books?id=eRcvAAAAQBAJ.

[34]. Ha iegan C, Gillich G-R, R duca E, Nedeloni M-D, Cîndea L. Equation of motion and determining the vibration mode shapes of a rectangular thin plate simply supported on contour using matlab. Analele Universitatii'Eftimie Murgu' 20 (1).

[35]. Shadnam M, Mofid M, Akin J. On the dynamic response of rectangular plate, with moving mass. Thin-Walled Struct. 2001;39(9):797–806.

[36]. Zellner A, Highfield RA. Calculation of maximum entropy distributions and approximation of marginalposterior distributions. J Econometrics 1988;37(2):195–209.

[37]. Shannon CE. A mathematical theory of communication. ACM SIGMOBILE Mob. Comput Commun Rev 2001;5(1):3–55.

[38]. Park SY, Bera AK. Maximum entropy autoregressive conditional heteroskedasticity model. J Econometrics 2009;150(2):219–30.

[39]. Drira S, Pai SG, Smith IF. Uncertainties in structural behavior for model-based occupant localization using floor vibrations. Front Built Environ 2021;7:13.

[40]. Reuland Y, Lestuzzi P, Smith IF. Data-interpretation methodologies for nonlinear earthquake response predictions of damaged structures. Front Built Environ 2017;3:43.

[41]. Gelman A, Carlin JB, Stern HS, Rubin DB. Bayesian data analysis. Chapman and Hall/CRC; 1995.

[42]. Kruschke JK. Posterior predictive checks can and should be bayesian: Comment on gelman and shalizi, "philosophy and the practice of bayesian statistics". Br J Math Stat Psychol 2013;66(1):45–56. [PubMed: 23003325]

[43]. Hodges JL. The significance probability of the smirnov two-sample test. Arkiv Mat 1958;3(5):469–86.

[44]. Chib S, Greenberg E. Understanding the Metropolis-Hastings algorithm. Amer Statist 1995;49(4):327–35.

[45]. Roberts GO, Rosenthal JS, et al. Optimal scaling for various Metropolis-Hastings algorithms. Statist Sci 2001;16(4):351–67.

[46]. Roberts GO, Smith AF. Simple conditions for the convergence of the gibbs sampler and Metropolis-Hastings algorithms. Stochastic Process Appl 1994;49(2):207–16.

[47]. Gelman A, Rubin DB. Inference from iterative simulation using multiple sequences. Statist Sci 1992;457–72.
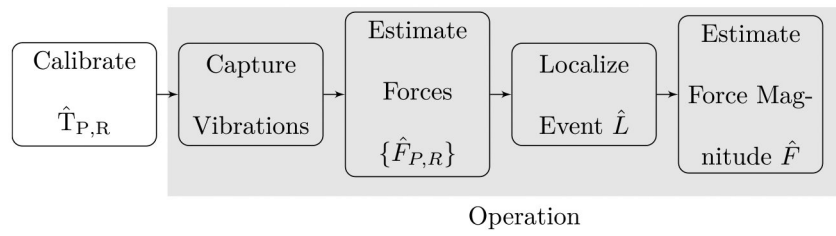
Fig. 1.
Force Estimation and Event Localization (FEEL) ([7,22]).
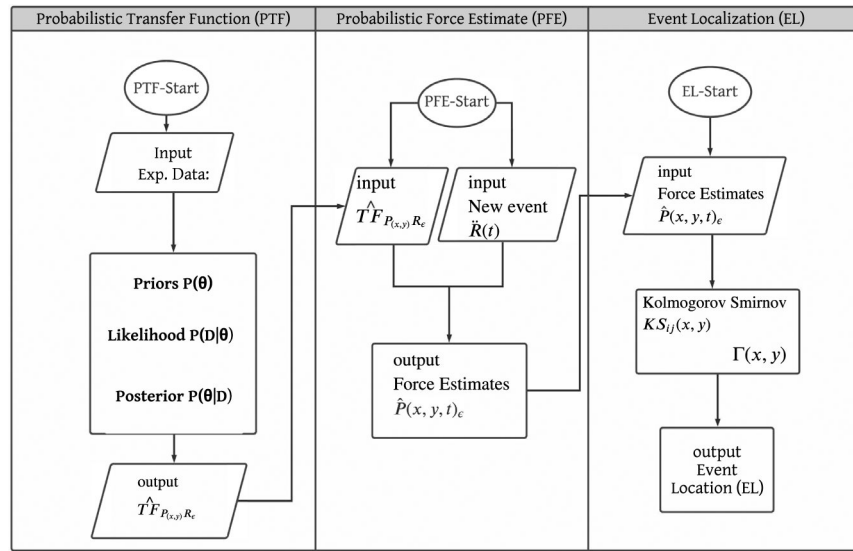
Fig. 2.
PFEEL algorithm design.
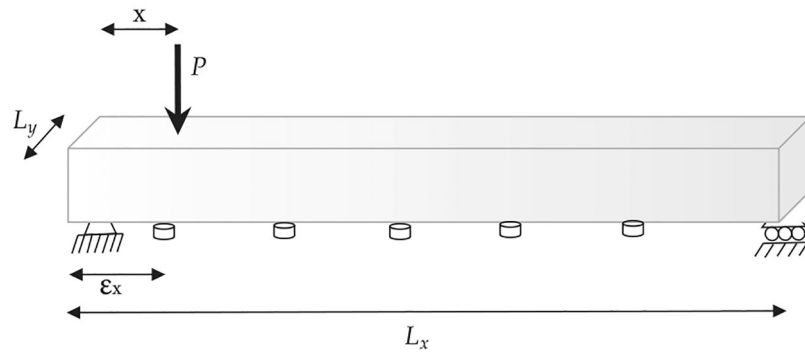
Fig. 3.
Simply supported beam.
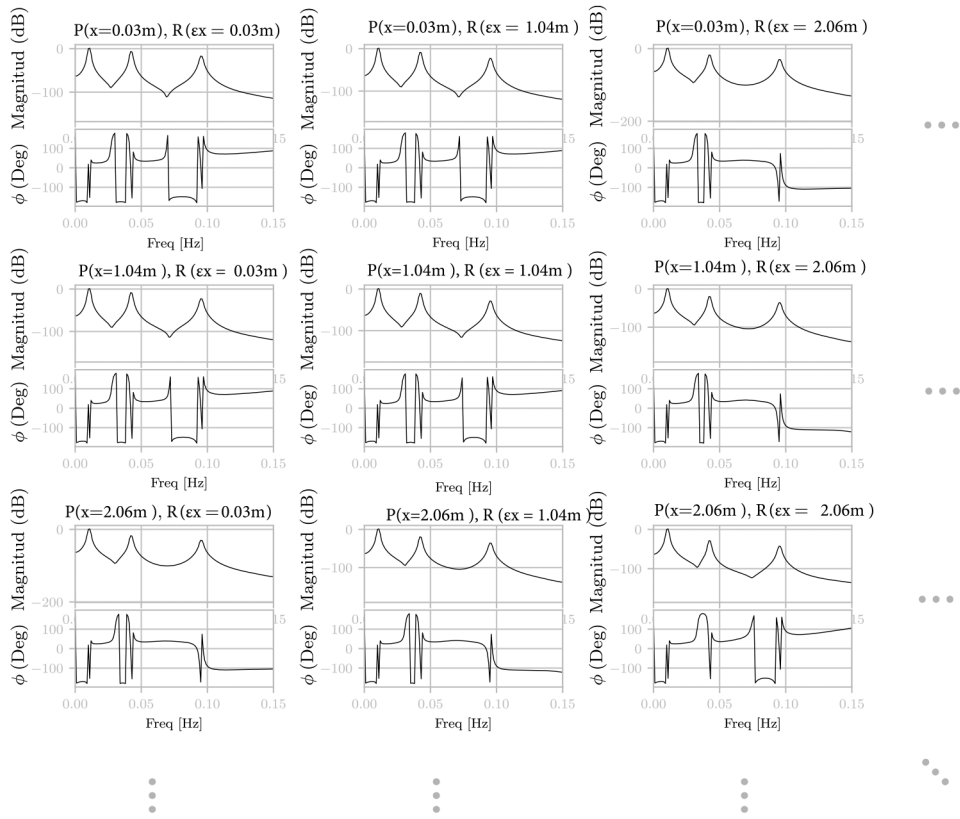
Fig. 4.
Magnitude and phase for representative $P_x - R_\epsilon$.
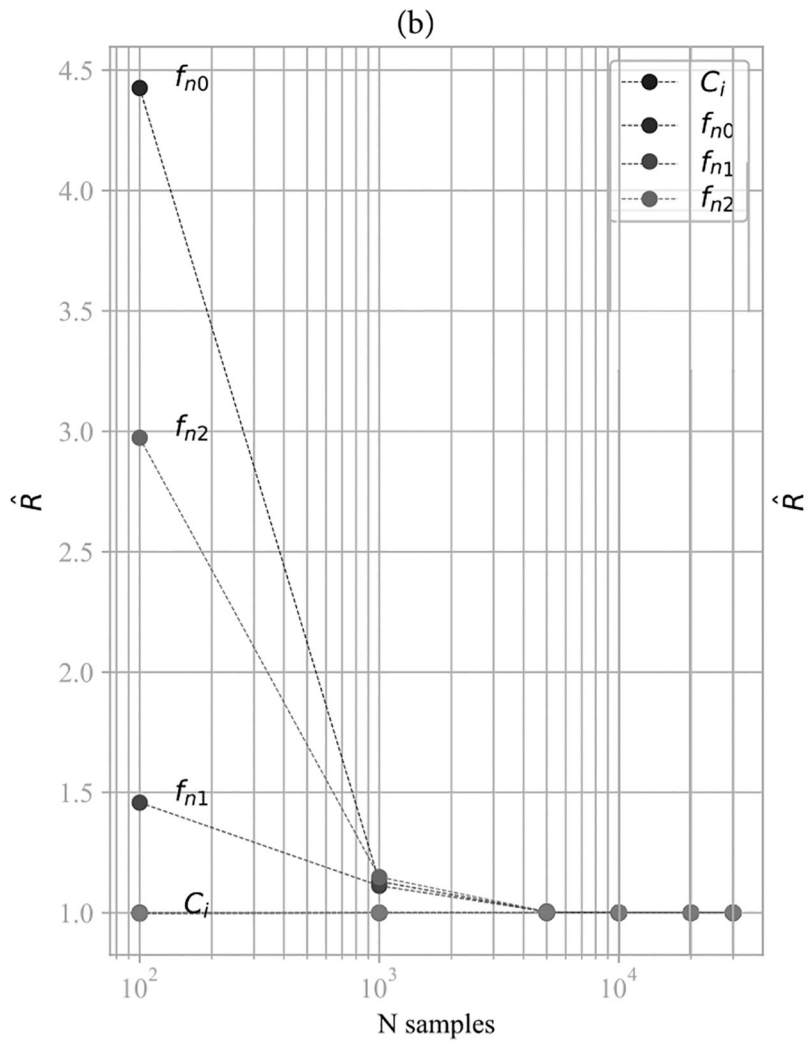
Fig. 5.
Convergence diagnostics using potential scale reduction factor for the random variables.
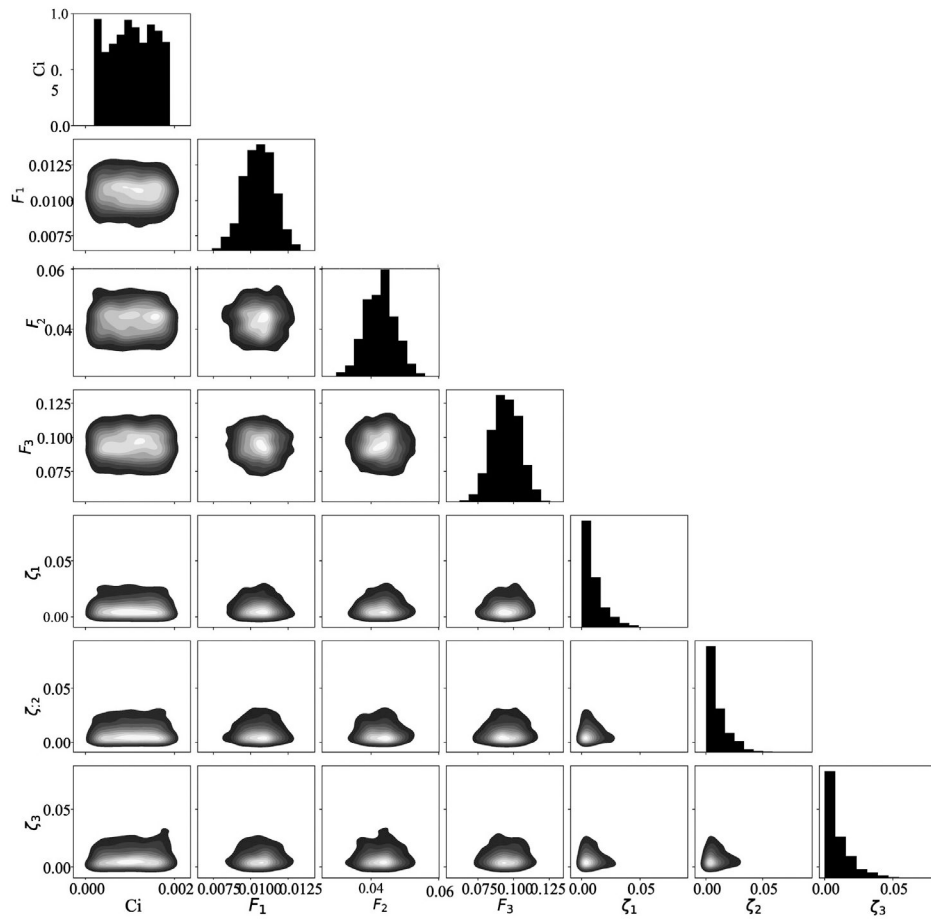
Fig. 6.
Diagonals represent the marginal posterior distributions of the model parameters, namely natural frequencies F_n, damping ratios ζ_n for three modes and shape constant C_i. The lower contours represent the joint posterior distribution.
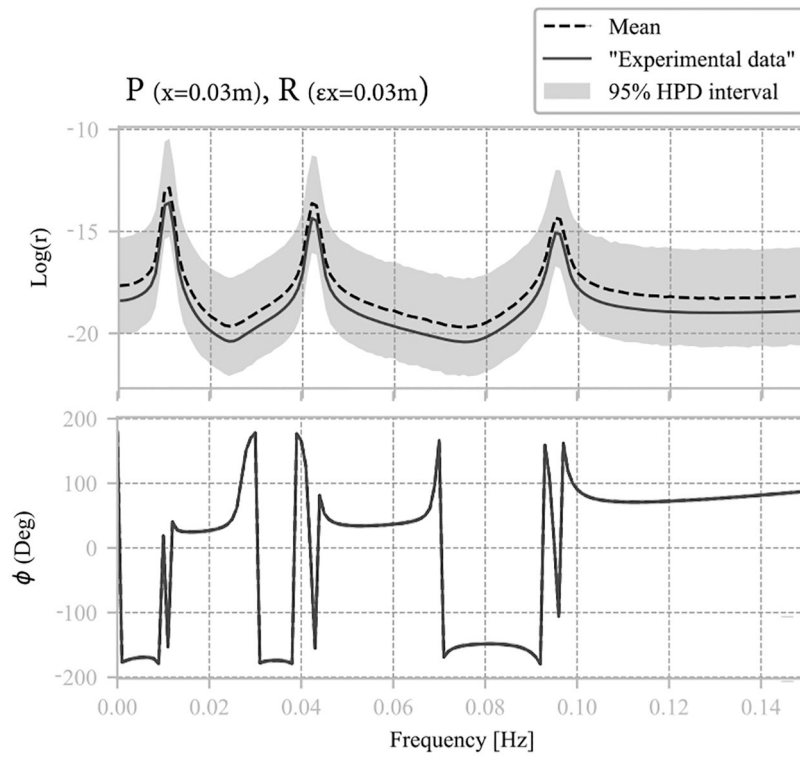
Fig. 7.
Goodness of fit test between experimental data and the probabilistic response for some P_x and R_{ϵ_x} at locations $x = 0.03$ and $x = 2.06$ m.
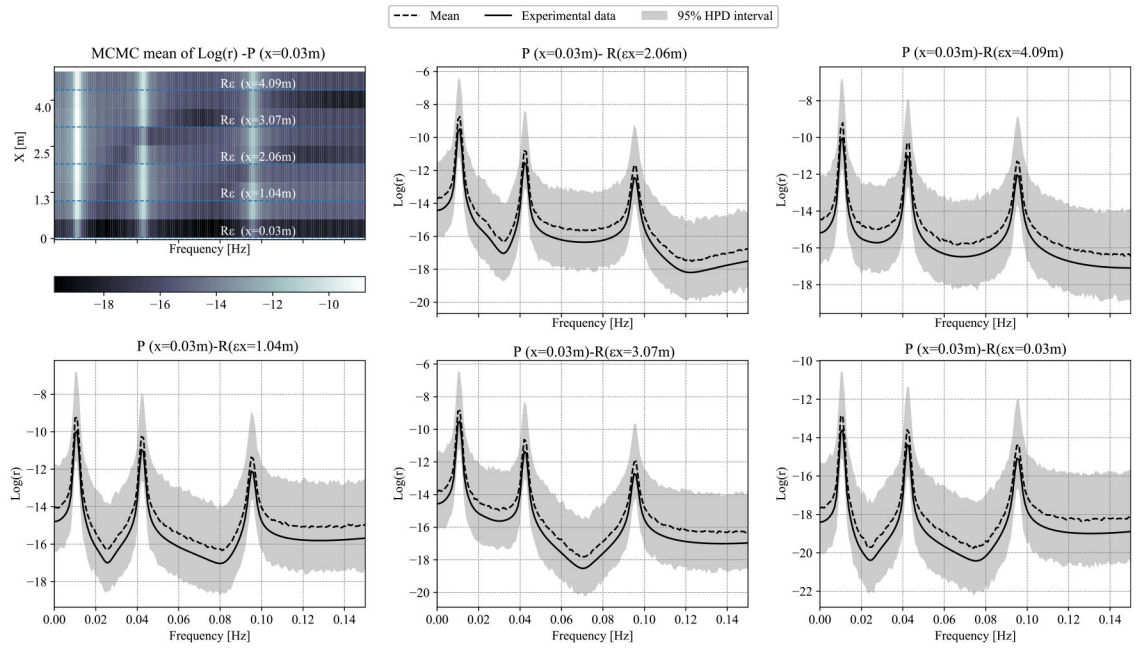
Fig. 8.
Goodness of fit test between experimental data and the probabilistic response for $P_{(x=0.03\text{ m})}$ and $R_{(\epsilon)}$.
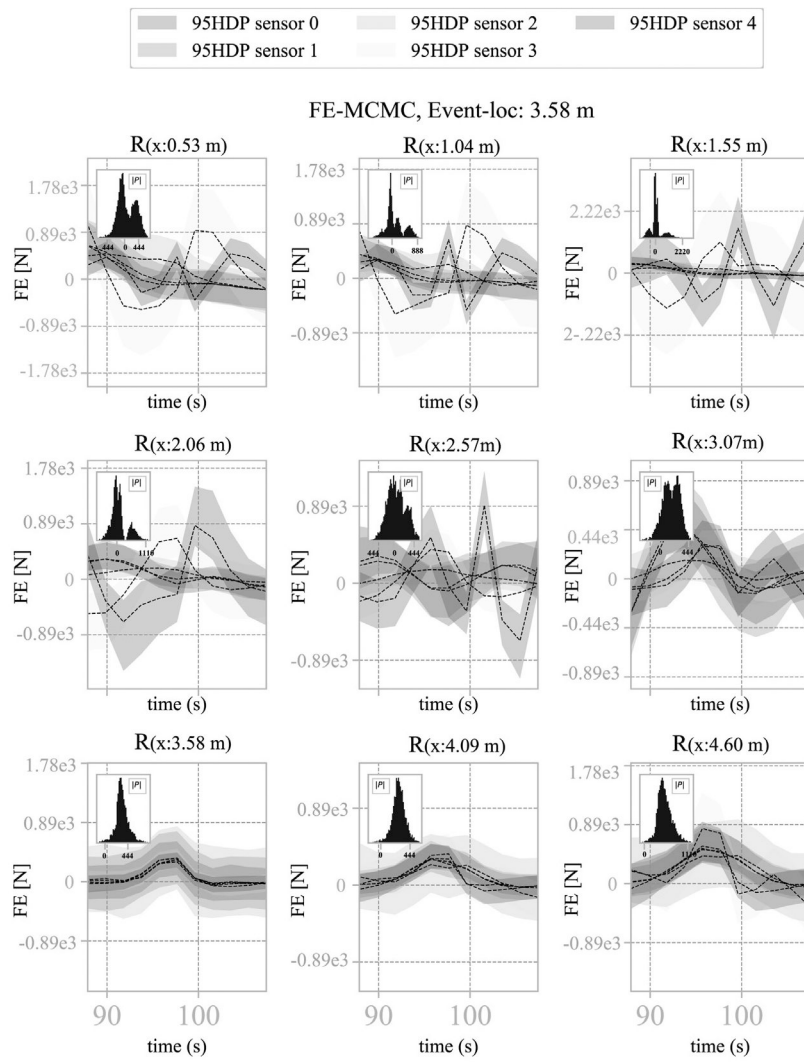
Fig. 9.
Force estimates for 10 different locations. The location of the event was $P_{(x=3.58\text{ m})}$.
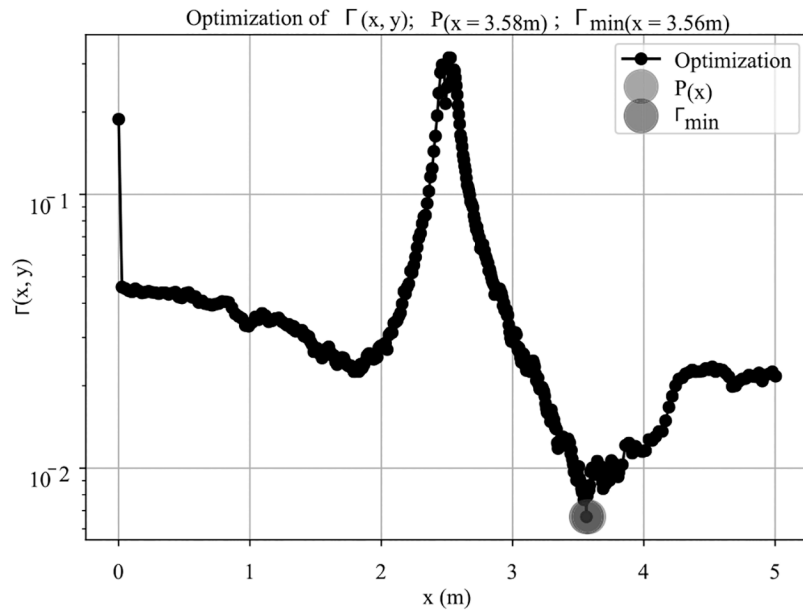
Fig. 10.
Optimization of $\Gamma_{(x, y)}$ for an impact at $P_{(x=3.58\ m)}$.
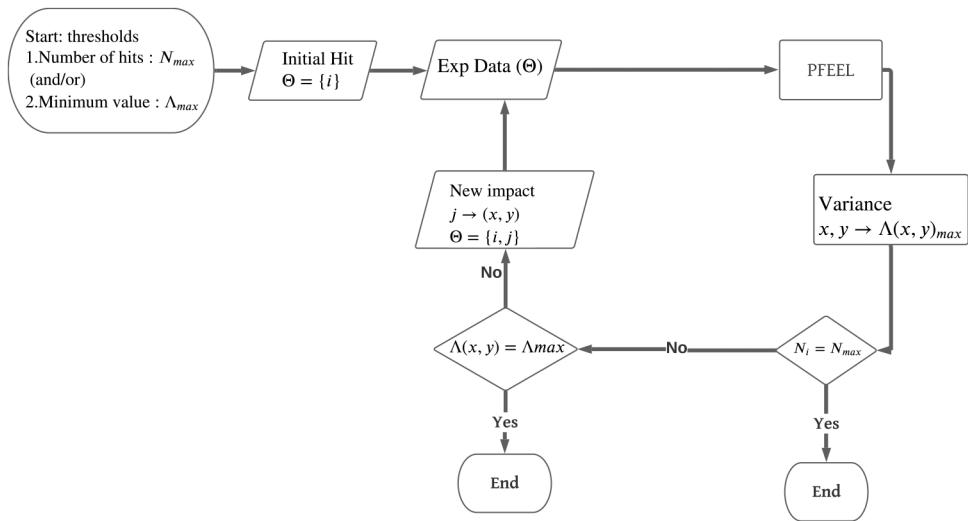
Fig. 11.
PFEEL-Calibration process.
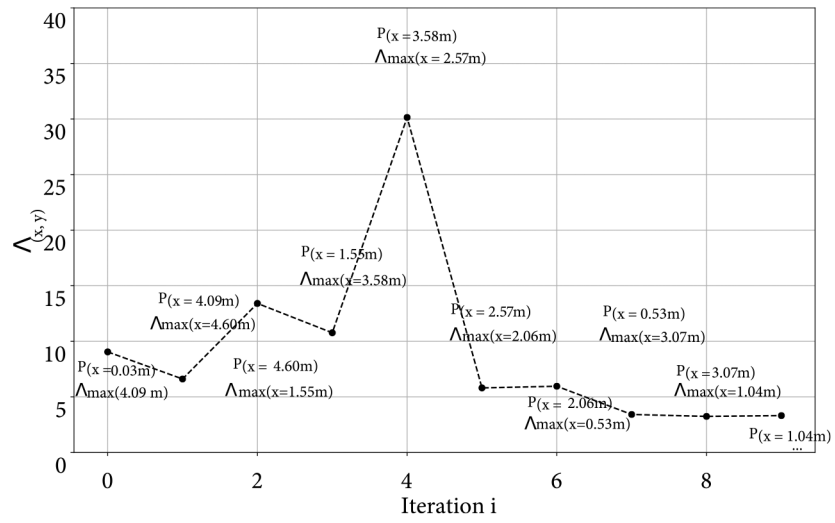
Fig. 12.
Maximization of $\Lambda(x, y)$.
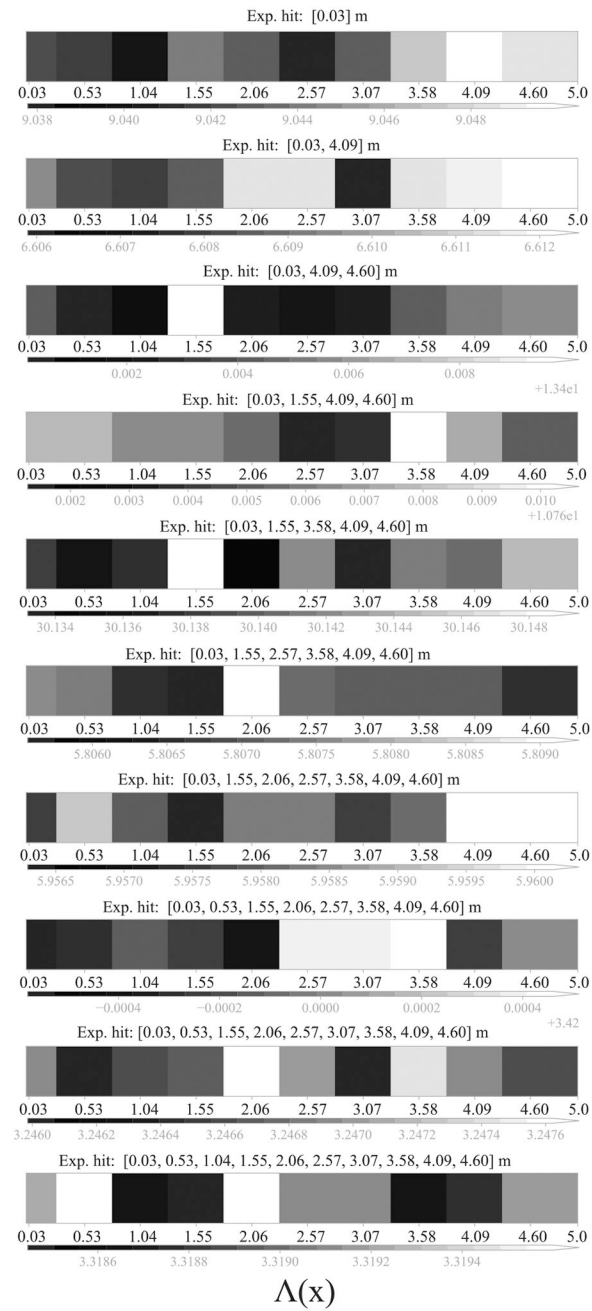
Fig. 13.
Extraction of the next hit location using Λ_{max} at each iteration.

Table 1

Beam model properties.

Young's modulus	E = 24.0 GPa
Unit weight	$2.40\text{e}3\ \frac{\text{Kg}}{\text{m}^3}$
Moment of inertia	$I = 8.99\text{e} - 05\ \text{m}^4$
Length	$L = 5.00\ \text{m}$
Area of the cross section	$A = 0.05\ \text{m}^2$